

## Scientific report

Regarding the project implementation in the period January–December 2021

Project title: “**The behaviour of new multicomponent polymeric systems in simulated environmental conditions for flame retardant coating materials**” Code: **PN-III-P1-1.1-TE-2019-0604**

### Stage Summary

The second stage of the project (2021) comprises three activities. The first activity consists of the obtaining and characterization of the semi-interpenetrating polymer networks (S-IPNs) based on the aromatic oligophosphonate (OP), previously synthesized and described in Stage 1 (2020 – Activity 1.3), and an epoxy resin (Activity 2.1). The second activity describes the microbiological testing of the S-IPNs (Activity 2.2). The third activity (Activity 2.3) describes the thermal and fire behavior of the S-IPNs. All proposed activities for this stage have been fully achieved and are presented below in this report.

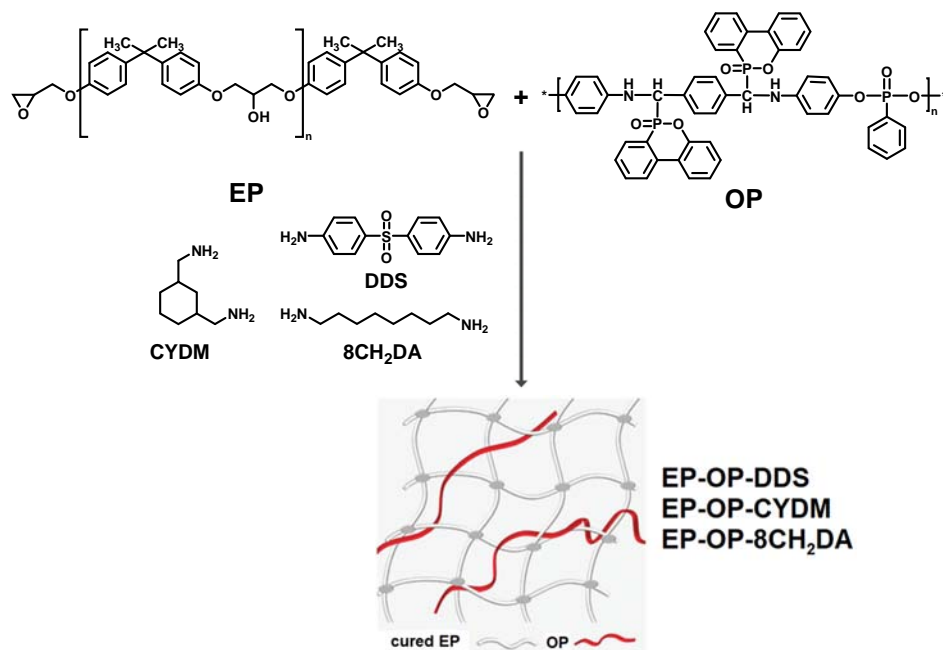
### Scientific and technical description

#### **Activity 2.1. The obtaining and characterization of the semi-interpenetrating polymer networks (S-IPNs) based on aromatic oligophosphonate (OP) and an epoxy resin**

Semi-interpenetrating polymer networks (S-IPNs) are related to other types of multicomponent polymeric materials (i.e. polymer blends, blocks and grafts), however having the advantage of crosslinking which permits exceptional control over the morphology. S-IPNs possess a unique structure comprised of a combination of at least two polymers situated in permanent entanglement and of which at least one is a crosslinked network [1,2]. Due to the characteristic structure formed during the synthesis of S-IPNs, there occurs a forced phase compatibilization through a synergistic effect on the entangled components. This leads to the enhancement of specific sought properties of the pristine comprising polymers. Consequently, S-IPNs possess a single glass transition temperature ( $T_g$ ) domain intermediate to the  $T_g$ s of the comprising components [3]. The advantages and disadvantages of epoxy resins have been presented in Stage 1 (2020 – Activity 1.1). Several recent strategies have been developed for improving the properties of epoxy resins. These include adding rubbers, thermoplastics and nanofillers [4–6]. Although these fillers significantly improved the toughness of epoxy resins, their presence reduces the thermal stability and the elastic modulus. The dispersion of the nanofillers into the epoxy matrix and increased system viscosity are other serious problems which must be addressed. These issues may be overcome by developing IPNs/S-IPNs which offer the advantages mentioned earlier. Moreover, some properties of the resulting material can be significantly improved with this strategy. For example, when polyphosphazene was introduced in the epoxy resin, it exhibited non-leaching behavior and enhanced flame retardancy, flexibility (low  $T_g$ ), oil/solvent resistance and biomedical compatibility [7]. Numerous studies on different flame retardant epoxy composites or blends containing phosphorus can be found in the literature. However, there exist limited literature on the introduction of different phosphorus containing flame retardant additives as linear components into epoxy S-IPNs [8].

##### **2.1.1. Obtaining and characterization of the S-IPNs**

The S-IPNs were obtained by mixing the epoxy resin, diglycidyl ether of bisphenol A (EP) with different amounts of OP under heating and stirring, followed by the curing in the presence of a suitable hardener (Table 1). The OP was previously synthesized and described in Stage 1 (2020 – Activity 1.3). 4,4'-diaminodiphenylsulfone (DDS), 1,3-bis(aminomethyl)cyclohexane (CYDM) and octamethylenediamine (8CH<sub>2</sub>DA) were used as curing agents for the epoxy resin to obtain three S-IPNs (Scheme 1). The epoxy to amine ratio was set at 2:1 based on the assumption that each hydrogen atom on the nitrogen atoms in the curing agents reacts with an epoxide ring. The quantity of OP was calculated in order to obtain final product with 2 wt% of phosphorus. The various formulations of the pre-curing mixtures are listed in Table 1. The required quantities of EP were mixed with OP under continuous stirring at 130 °C until complete dissolution was achieved followed by the addition of a hardener and cooling of the mixture to 80 °C. The resulting mixtures were stirred homogeneously and poured into a Teflon coated mould to obtain the samples in the shape of plates. The formulation based on DDS was cured at 150 °C for 2 h and 180 °C for 3 h. The rest of the samples were cured at 70 °C for 4 h, 130 °C for 2 h and 150 °C for 1 h. Finally, the thermosets were cooled slowly to room temperature to prevent cracking.



**Scheme 1.** Obtaining of the cured matrices and S-IPNs.

**Table 1.** Composition of the samples.

Sample	Hardener	Hardener (g)	Oligophosphonate (OP) (g)	Epoxy resin (EP) (g)
EP-DDS	DDS	7.45	-	22.55
EP-OP-DDS	DDS	5.99	5.61	18.36
EP-CYDM	CYDM	4.66	-	25.34
EP-OP-CYDM	CYDM	3.79	5.56	20.63
EP-8CH <sub>2</sub> DA	8CH <sub>2</sub> DA	4.79	-	25.23
EP-OP-8CH <sub>2</sub> DA	8CH <sub>2</sub> DA	3.87	5.65	20.50

where: EP-OP-DDS, EP-OP-CYDM and EP-OP-8CH<sub>2</sub>DA are the S-IPNs and EP-DDS, EP-CYDM and EP-8CH<sub>2</sub>DA the cured matrices without the OP

The structural investigations of the S-IPNs were undertaken by Fourier transform infrared spectroscopy (FTIR) and scanning electron microscopy (SEM) coupled with energy dispersive X-ray spectroscopy (EDX).

**FTIR:** The FTIR spectra of the S-IPNs are given in Figure 1a. The OP component exhibited a sharp absorption band at 1477 cm<sup>-1</sup> describing the aromatic P-C stretching vibrations. The bands from 1202, 1045 and 922 cm<sup>-1</sup> correspond to P-O-C stretching vibrations. According to the literature the weak signals region 1040–910 cm<sup>-1</sup> of the samples spectra describe stretching vibrations of P-OH bond in O=P-OH from the end-capping of the low content OP in the networks [9]. The band at 1203 cm<sup>-1</sup> corresponds to aromatic P=O stretching. The deformation vibrations of 1,2-disubstituted aromatic DOPO rings generate the band at 754 cm<sup>-1</sup>, while the band at 825 cm<sup>-1</sup> is characteristic to the deformation vibrations of p-phenylene rings [10]. The signals at 1608 and 1508 cm<sup>-1</sup> correspond to aromatic C=C stretching vibrations. The EP is mainly characterized by the signal localized at 915 cm<sup>-1</sup> specific to the epoxy ring and the signals from 1598 and 1511 cm<sup>-1</sup> characteristic to skeletal C=C vibrations in aromatic moieties. In addition, the region 1000–1300 cm<sup>-1</sup> describes aryl alkyl ether moieties [11]. These signals also appear in the FTIR spectra of the S-IPNs. The group of signals around 2963 cm<sup>-1</sup> and 2928 cm<sup>-1</sup> correspond to aliphatic C-H asymmetric stretching vibrations, while the one around 2850 cm<sup>-1</sup> is attributed to aliphatic C-H symmetric stretching vibrations. The broad band around 3502 cm<sup>-1</sup> in the FTIR spectrum of EP corresponds to O-H stretching vibrations. Upon curing the EP matrices, the epoxide ring is cleaved resulting more O-H entities and N-H stretching vibrations appear from secondary amines. Thus, the region 3000–4000 cm<sup>-1</sup> (with a peak at around 3400 cm<sup>-1</sup>) becomes much broader and intense in FTIR spectra of the S-IPNs, as one may see in Figure 1. The opening of the epoxy ring was further confirmed by the absence of its characteristic absorption bands in the S-IPNs spectra: the band at 3056 cm<sup>-1</sup> (C-H stretching vibrations of methylene in the epoxy ring) and the band from 915 cm<sup>-1</sup>. Furthermore, the bands at 1172 and at 1225 cm<sup>-1</sup> correspond to the secondary

amines, demonstrating the formation of C–N bonds after the epoxide ring opening with the diamines [10]. The S–IPNs exhibited important signals, such as the one at  $1475\text{ cm}^{-1}$ , corresponding to stretching vibrations of aromatic P–C bond. The signals at  $1044\text{ cm}^{-1}$  and  $932\text{ cm}^{-1}$  are attributed to P–O–C bond stretching vibrations. The signals at  $754$  and  $715\text{ cm}^{-1}$  are due to deformation vibrations of the 1,2–disubstituted aromatic DOPO and aromatic rings of the DDS curing agent in EP–OP–DDS. The presence of all these signals successfully confirms the obtaining of the S–IPNs [9].

**SEM–EDX:** Figure 1b shows the SEM micrographs of the samples fracture surfaces obtained after cooling in liquid nitrogen. The micro fractures are spread within the entire S–IPNs sample masses, the minimal fracture area occurring through crack propagation. The uniform fractures were generated during thermal treatment by OP agglomerates, behaving as stress concentration centres and indicating a good homogeneous dispersion of the OP into the cured epoxy matrices [12]. Moreover, the reactive epoxide rings of the resin are crosslinked to generate larger chains, indicating that the curing agents are well distributed within the whole matrix. The EDX analysis confirmed the presence of low content phosphorous from OP in the S–IPNs (Figure 1c).

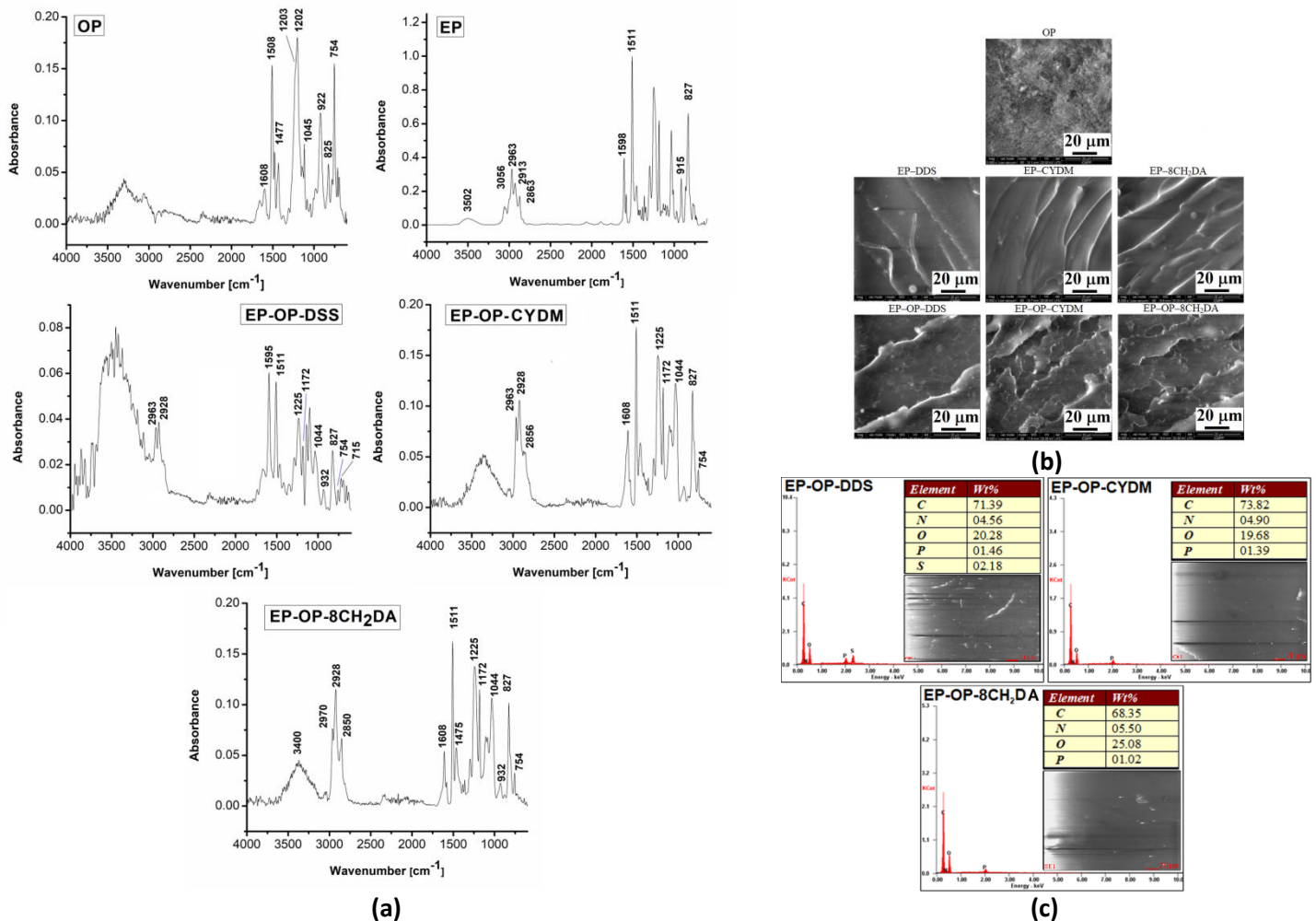


**Figure 1.** FTIR spectra (a), SEM micrographs (b) and EDX analysis (c) of the S–IPNs.

### Activity 2.2. The microbiological testing of the S–IPNs

Since the S–IPNs are intended as future wood protective coatings, the samples microbiological resistance was tested against three wood decaying fungal strains: *Penicillium chrysogenum* ATCC10106, *Cladosporium cladosporioides* ATCC16022 and *Aspergillus brasiliensis* ATCC 9642. In our case, the assessment of degradation degree after 10 weeks of exposure was based on visual observations. As it may be observed from Figure 2, during the decay test all surfaces of samples were not covered by the fungal colonies, except samples exposed to *A. brasiliensis* where the edges were slightly covered.

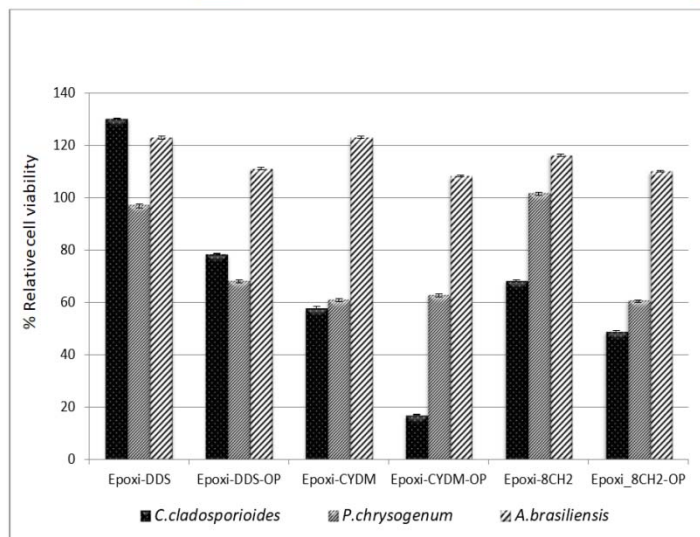
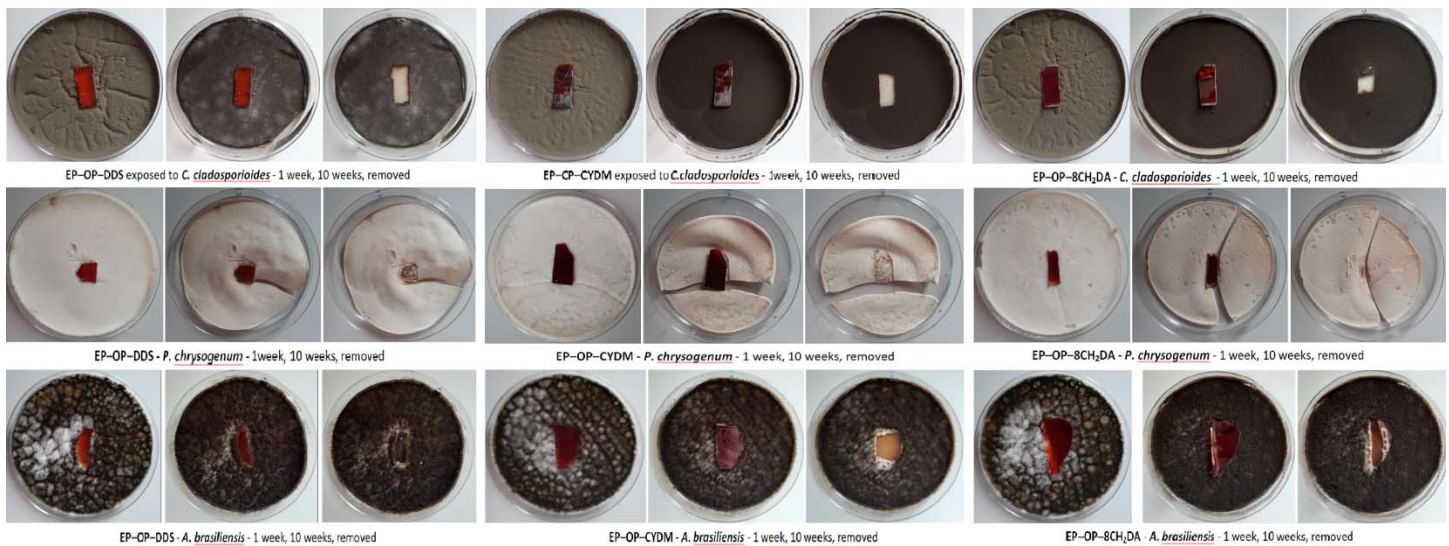


**Figure 2.** Microbiological testing of the networks.

Even if there was not distinguished a notable growth of the colonies on the samples, the fungicidal properties when compared with a control varied (Figure 2). The sample encoded EP-OP-CYDM reduced the population of *P. chrysogenum* at 17 %. Not so promising results were obtained in case of the samples incubated with *A. brasiliensis*, where there was not noticed a fungicidal activity for none of the tested samples. Also it was noticed that the S-IPNs had a greater fungicidal activity than their cured counterparts without OP, due to the presence of phosphorus. The samples presented instead fungicidal properties when incubated with *C. cladosporioides* and *A. brasiliensis* and partially for *P. chrysogenum*, the areas under the samples remaining clear of fungal colonies after 10 weeks of incubation where the samples adhered perfectly to the culture media (Figure 2).

### Activity 2.3. The thermal and fire behavior of the S-IPNs

#### 2.3.1. Differential scanning calorimetry (DSC) and comparative thermal degradation studies in inert and thermo-oxidative atmospheres by thermogravimetric analysis (TGA)

##### 2.3.1.1. DSC study

Assessment of thermal stability of materials for high temperature applications is crucial and resides in the evaluation of some essential parameters: the temperature corresponding to 5 % mass loss ( $T_{5\%}$ ), the temperature at which the mass loss rate is the highest ( $T_{max}$ ), mass residue remaining after thermal degradation (700 °C) and the  $T_g$ . The thermal behavior of the S-IPNs, OP and crosslinked matrices was evaluated. All structures exhibited a single neat  $T_g$  domain (Figure 3). The OP showed a  $T_g$  value at 132 °C. No other thermal transitions were observed, hence no further crosslinking expected to occur. The presence of a single  $T_g$  domain is a sign of good compatibility between components within the S-IPNs. It is a known fact that the obtaining of S-IPNs induces a forced phase compatibilization through a synergistic effect of the comprising components, based on compatible polarities [13]. One may also observe from the DSC data that the  $T_g$  values of the S-IPNs are situated between those of the OP and their corresponding cured matrices. This is an indication that the S-IPNs were successfully obtained [13]. The bulky aromatic DOPO entities in OP generate a steric hindering effect, leading to an increase in S-IPNs  $T_g$  values compared to their corresponding crosslinked EP matrices, except for the sample cured with DDS. In this case, the presence of OP had a strong plasticizing effect which led to a significant reduction in the  $T_g$  value from 201 °C (EP-DDS) to 141 °C (EP-OP-DDS). This is due to the increase in free volume between segmental chains and hence their mobility, which is also dictated by the bulky aromatic nature of the curing agent, as also found for other S-IPN epoxy systems, making the material adequate for applications which require lower  $T_g$  values [12].

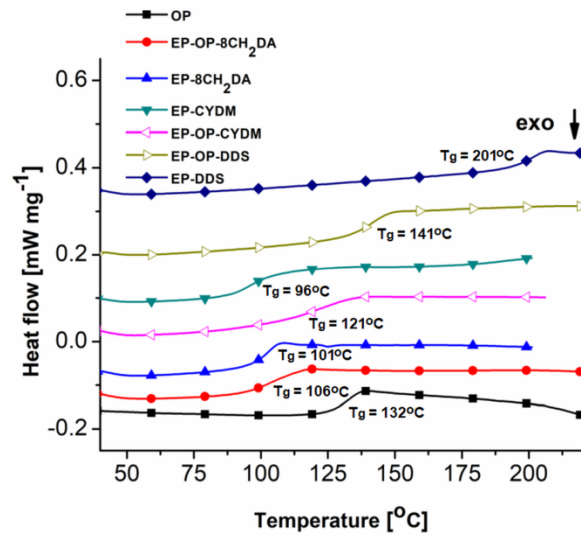


Figure 3. DSC curves of the OP and networks.

### 2.3.1.2. TGA studies in inert and thermo-oxidative atmospheres

The phosphorus influence on the thermal stability of the structures was investigated with the aid of TGA and first derivative curves (DTG) in both inert and air atmospheres. The main data extracted from the thermal measurements are shown in Figure 4 and Table 2.

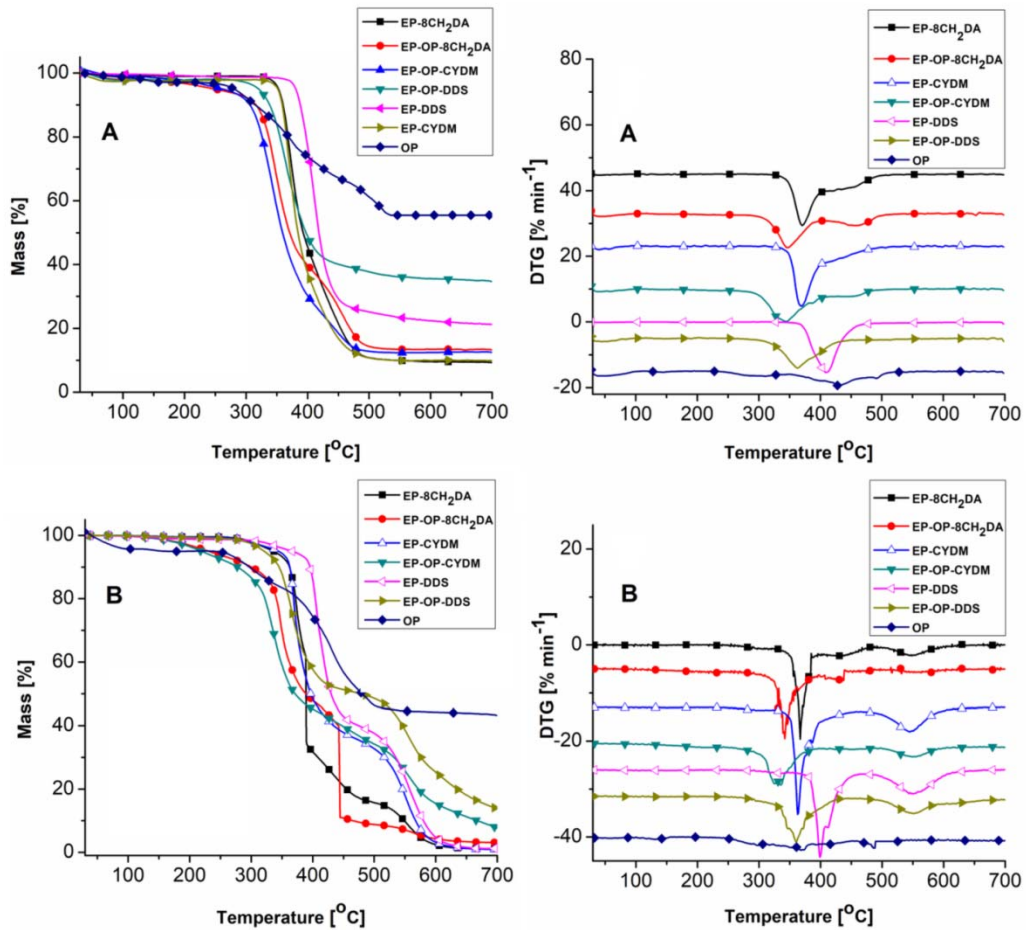


Figure 4. TGA (left) and DTG curves (right) in (A) nitrogen and (B) air.

**Table 2.** Thermal properties of the structures.

Sample	Atm.	Thermal degradation stages					$T_{\text{endset}}$ (°C)	$T_{\text{endset}} - T_{5\%}$ (°C)	R (%)	$T_g$ (°C)
		$T_{5\%}$ (°C)	$T_{\text{max}1}$ (°C)	$T_{\text{max}2}$ (°C)	$T_{\text{max}3}$ (°C)	$T_{\text{max}4}$ (°C)				
OP	Air	258	297	372	418	485	510	252	43.28	–
	N <sub>2</sub>	275	311	395	430	491	530	255	55.5	132
EP–DDS	Air	359	400	550	–	–	600	241	1.25	–
	N <sub>2</sub>	381	410	–	–	–	450	69	21.21	201
EP–OP–DDS	Air	315	360	550	–	–	575	260	13.31	–
	N <sub>2</sub>	321	363	387	–	–	410	89	34	141
EP–CYDM	Air	339	364	546	–	–	590	251	1.02	–
	N <sub>2</sub>	352	370	437	–	–	460	108	9.75	96
EP–OP–CYDM	Air	213	335	552	–	–	580	367	7.13	–
	N <sub>2</sub>	262	344	387	458	–	473	201	12.26	121
EP–8CH <sub>2</sub> DA	Air	330	300	370	550	–	590	260	1.11	–
	N <sub>2</sub>	352	371	435	–	–	475	123	9.26	101
EP–OP–8CH <sub>2</sub> DA	Air	225	340	435	555	–	587	362	3.07	–
	N <sub>2</sub>	249	347	462	–	–	485	236	13.04	106

$T_{5\%}$  – temperature corresponding to 5 % mass loss;

$T_{\text{max}}$  – temperature corresponding to the highest mass loss rate per each thermal degradation stage;

$T_{\text{endset}}$  – temperature corresponding to the endset of thermal degradation;

R – residue mass remained at 700 °C;

$T_g$  – glass transition temperature.

In both atmospheres the individual linear component, OP, underwent a complex thermal decomposition process in four overlapping stages. In an inert atmosphere (N<sub>2</sub>), the OP exhibited a 5 % mass loss temperature ( $T_{5\%}$ ) value of 275 °C and a multi-step decomposition pattern with maximum decomposition temperature ( $T_{\text{max}}$ ) values of 311 °C, 395 °C, 430 °C, 491 °C, a thermal degradation endset temperature ( $T_{\text{endset}}$ ) of 530 °C and a final stable residue (R) of 55.5 %. As expected, the presence of oxygen accelerated the thermal degradation of the OP in air, resulting in lower characteristic temperatures ( $T_{5\%} = 258$  °C;  $T_{\text{max}} = 297$  °C, 372 °C, 418 °C, 485 °C;  $T_{\text{endset}} = 510$  °C) and R value (43.28 %).

In nitrogen atmosphere the aromatic nature of the DDS curing agent endowed the crosslinked epoxide matrix (EP–DDS) with the highest thermal stability of all the investigated materials ( $T_{5\%} = 381$  °C), decomposing in a single stage ( $T_{\text{max}} = 410$  °C) and yielding 21.21 % residue. By comparison to EP–DDS, the cycloaliphatic and aliphatic hardeners exhibited additional thermal decomposition (overlapping) stages and decreased thermal stability. The corresponding cured epoxy matrices (EP–CYDM, EP–8CH<sub>2</sub>DA), exhibit  $T_{5\%} = 352$  °C and lower almost identical residues of 9.75 % (EP–CYDM) and 9.25 % (EP–8CH<sub>2</sub>DA), respectively. The TGA residues increased for OP containing S–IPNs to 34 % for EP–OP–DDS, 12.26 % for EP–OP–CYDM and 13.04 % for EP–OP–8CH<sub>2</sub>DA. The increased char formation of OP blocks the release of volatile products due to the solid phase action of the phosphorus. The S–IPNs thermal stabilities were also dictated by the chemistry of the curing agent (EP–OP–DDS > EP–OP–CYDM > EP–OP–8CH<sub>2</sub>DA). The S–IPNs containing OP exhibit lower  $T_{5\%}$  values which could be due to catalyzed decomposition caused by phosphorus based acidic species. In addition, during the formation of the S–IPNs there occur hydrogen bonds disruptions in both the OP and epoxy resin when the OP gets trapped within the crosslinked epoxy network during curing. This aspect, together with the lower thermal stability of OP, due to the more thermally labile P–C bond in the additive, leads to the decrease of  $T_{5\%}$  in the S–IPNs below that of the neat OP. Rosu et al. [14] correlated the broadening of the  $T_{\text{endset}} - T_{5\%}$  range with surface compactness during thermal degradation leading to decrease in volatiles evolution. The same is observed in the case of this study. The obtained S–IPNs are more compact than their comprising components, because a decrease in the rate of volatiles evolution due to the significant broadening of the range  $T_{\text{endset}} - T_{5\%}$  of the S–IPNs by comparison to their crosslinked matrices without OP (Table 2).

The TGA measurements undertaken in air showed that the presence of oxygen led to a more complex degradation mechanism of the epoxy samples. This explains the very high differences in char yield between the two working atmospheres, in air being lower. Regardless of the working atmosphere, the  $T_{5\%}$  and  $T_{\text{max}}$  values of S–IPNs were generally lower than those of the cured epoxy matrices, due to the lower thermal resistance of the P–C bond [15].

### 2.3.2. Determination of non-isothermal kinetic parameters of thermal degradation

The undertaking of the thermal kinetic studies was in accordance with the recommendations of the International Confederation on Thermal Analysis and Calorimetry (ICTAC) [16]. In Figure 5 there are shown the TGA and DTG curves registered at 10, 20, 30 °C min<sup>-1</sup> heating rates under nitrogen atmosphere for the S-IPNs. Using the TGA curves at three heating rates and the Friedman (FR) and Ozawa-Flynn-Wall (OFW) equations included in the “Netzsch Thermokinetics-3” software the initial kinetic thermal degradation parameters were calculated. Figure 5 shows that with the increase of the heating rate, the TG curves shift to higher temperatures due to temperature delay as a function of heating rate [17,18]. The data in Tables 2 and 3, the DTG curve shapes and the variation of activation energy ( $E_a$ ) with the conversion degree ( $\alpha$ ) (Figure 6) show that the degradation processes follow complex mechanisms in multiple reactions: consecutive, parallel or competitive [19,20].

The fact that the degradation processes are complex requires the use of the multiple linear regression (MLR) method to identify the degradation mechanisms. MLR assumes that the parameters of the kinetic model are identical for all measurements. Using an iterative method, the software numerically resolves the differential equations of some reaction models (18 reaction mechanisms) [21,22] for  $\alpha$  in the range 0.1 – 0.85, calculating the minimum value of least squares between simulated and the experimental data, suggesting the best kinetic model for the thermal degradation process. The most probable kinetic model was chosen based on visual appreciation and of statistics coefficients (the experimental F-value ( $F_{exp}$ ),  $F_{crit}$  (0.95) and correlation coefficients). In the present case the successive processes take place in two and three steps and were assigned to the schemes (1) and (2) (Table 3):



with the following types of process mechanisms: d:f; An,Fn, for EP-OP-8CH<sub>2</sub>DA and EP-OP-DDS and t:f,f; An, Fn, Fn for EP-OP-CYDM. A is the solid initial product, B is the intermediate products (solid, liquid or gaseous) and C/ D is the final solid residue. The numbers 1, 2, 3 represent the reaction steps.

The next conversion functions for one single step were used:

-Avrami-Erofeev reaction model An:

$$f(\alpha) = n(1 - \alpha)[ -\ln(1 - \alpha)] \quad (3)$$

where n is a constant parameter.

- n<sup>th</sup> reaction order model Fn:

$$f(\alpha) = (1 - \alpha)^n \quad (4)$$

where n is the reaction order and  $\alpha$  is the conversion degree;

Using the kinetic parameters presented in Table 3, the TGA curves can be recalculated (between 200 and 550 °C). These recalculated curves approximate well the experimental data, suggesting that the obtained theoretical models accurately simulate the real thermal degradation phenomenon (Figure 5).

As seen in Table 3, for all samples, in the majority of degradation stages the reaction order has values greater than 1. This fact suggests that during the degradation processes higher molecular weight products may appear [23].

$E_a$  and the pre-exponential factor (logA) differ depending on the chemical structure of the curing agents. The activation energies vary between 190 and 250 kJ mol<sup>-1</sup> for the samples cured with aliphatic hardeners and between 219 and 242 kJ mol<sup>-1</sup> for the sample cured with aromatic hardener. The total  $E_a$  assigned to the entire thermal decomposition process is the sum of the  $E_a$  values for each step.

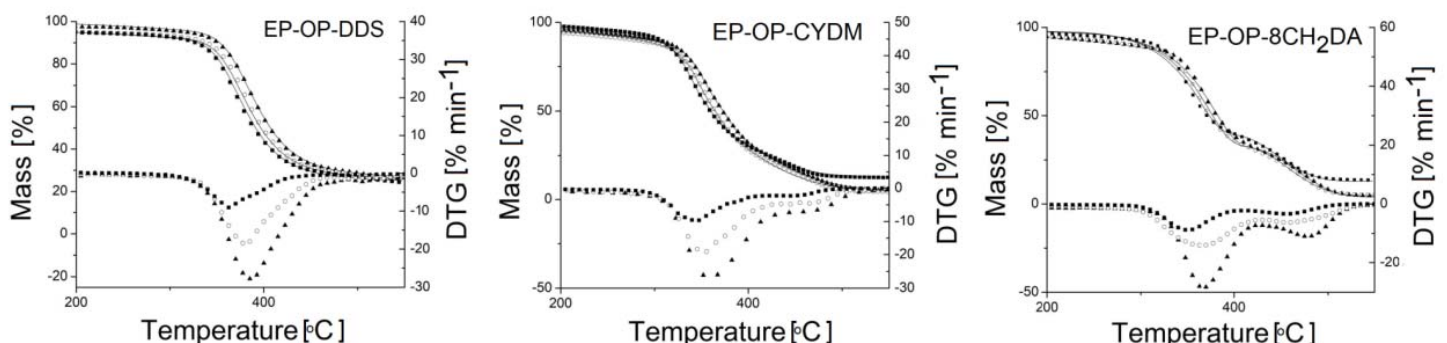


**Figure 5.** TG and DTG curves registered at: (■) 10, (○) 20, (▲) 30 °C min<sup>-1</sup> heating rates. The continuous line represents experimental curves. Symbols represent software simulated curves.

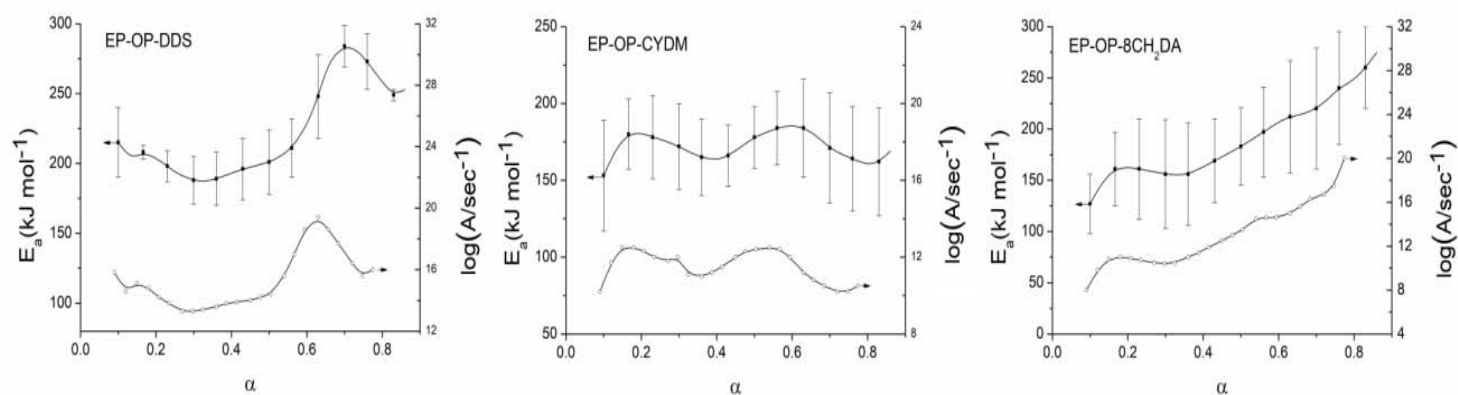


**Figure 6.** Variation of kinetic parameters with conversion degree.

**Table 3.** Kinetic and statistics parameters determined after non-linear regression for the most probable mechanism of thermal degradation process of the S-IPNs products by applying a kinetic model in two and three steps, with consecutive reactions in the temperature interval 100–550 °C.

Parameters	EP-OP-DDS	EP-OP-CYDM	EP-OP-8CH <sub>2</sub> DA
	d:f; An,Fn	t:f,f; An,Fn,Fn	d:f; An,Fn
	mechanism scheme	mechanism scheme	mechanism scheme
	A-1 → B-2 → C	A-1 → B-2 → C-3 → D	A-1 → B-2 → C
$E_1$ /kJmol <sup>-1</sup>	242	196	221
log $A_1$ /s <sup>-1</sup>	15.85	14.03	20.76
$n_1$	0.338	0.215	0.245
$E_2$ /kJmol <sup>-1</sup>	219	219	190
log $A_2$ /s <sup>-1</sup>	16.17	16.45	14.03
$n_2$	2.661	0.973	3.536
$E_3$ /kJmol <sup>-1</sup>	-	250	-
log $A_3$ /s <sup>-1</sup>	-	19.89	-
$n_3$	-	1.384	-
folReact 1	0.8245	0.216	0.112
folReact 2	-	0.690	-
Fexp	1.00	1.00	1.00
Fcrit-0.95.	1.19	1.16	1.196
t-critical(0.95)	1.956	1.956	1.956
correl-coeff	0.999017	0.999883	0.999527

$E_1, E_2, E_3$  – represent the activation energies of thermal degradation for each step; log ( $A_1, A_2, A_3$ ) are the pre-exponential factors for each step;  $n_1, n_2, n_3$  are the reaction order for each step; logKcat1 is the autocatalytic constant for the reaction step 1; folReact 1 is the share from the total process for the reaction step 1 (A→B); folReact 2 is the share from the total process for the reaction step 2 (B→C) and the share of step 3 (C→D) in the total process, is given by  $1 - \sum(\text{folReact})$



### 2.3.3. Evolved gases analyses by TGA–FTIR and Py–GC–MS

#### 2.3.1.1. TGA–FTIR

TGA–FTIR coupling was used to study the evolved gaseous mixtures formed during the thermal degradation of the epoxy samples. The FTIR spectra of volatiles released from the decomposition of OP and S–IPNs at relevant  $T_{\max}$  values (Table 2) are presented in Figure 7. The weak signal at  $3059\text{ cm}^{-1}$  in the FTIR spectra for OP is associated with the aromatic C–H stretching vibration, as well as the signal  $3011\text{--}3016\text{ cm}^{-1}$  are found in all spectra [24]. The peaks at  $3086\text{ cm}^{-1}$  and  $3113\text{ cm}^{-1}$  correspond to N–H from amine moieties. The broad signal in the range  $3500\text{--}3000\text{ cm}^{-1}$  with a peak at  $\sim 3250\text{ cm}^{-1}$ , present in all spectra, corresponds to O–H bond stretching vibrations of alcohol moieties and/or carboxylic acids. Signals corresponding to aliphatic C–H asymmetric and symmetric stretching vibrations observed ( $\sim 2959\text{ cm}^{-1}$  and  $\sim 2937\text{ cm}^{-1}$ ) could be due to different moieties, including fractions containing  $\text{CH}_3$ . The signals from  $1500\text{--}1600\text{ cm}^{-1}$  and  $690\text{--}669\text{ cm}^{-1}$  confirm the presence of entities with aromatic structures. The peak at around  $\sim 2360\text{ cm}^{-1}$  also appears in all spectra and is ascribed to  $\text{CO}_2$  evolution, together with the range  $4000\text{--}3500\text{ cm}^{-1}$ , associated with water. The signals in the range  $1200\text{--}2000\text{ cm}^{-1}$  contain overlapping absorption bands from: vibrations of C=O, C=C, water, cycloaliphatic structures, P–Ar stretching vibrations ( $\sim 1420\text{ cm}^{-1}$ ), P=O stretching vibrations ( $\sim 1185\text{ cm}^{-1}$ ), ketone stretching vibrations ( $\sim 1690\text{--}1747\text{ cm}^{-1}$ ). The decarboxylation reaction and scission of the different carbonyl groups lead to the formation of  $\text{CO}_2$ . Additional bands at around  $1600$  and  $1509\text{ cm}^{-1}$  correspond to C=C stretching vibration of aromatic rings. The absorption bands around  $3000\text{ cm}^{-1}$  describe the  $\text{sp}^2$  and  $\text{sp}^3$  C–H stretching vibrations of aromatic and aliphatic species.

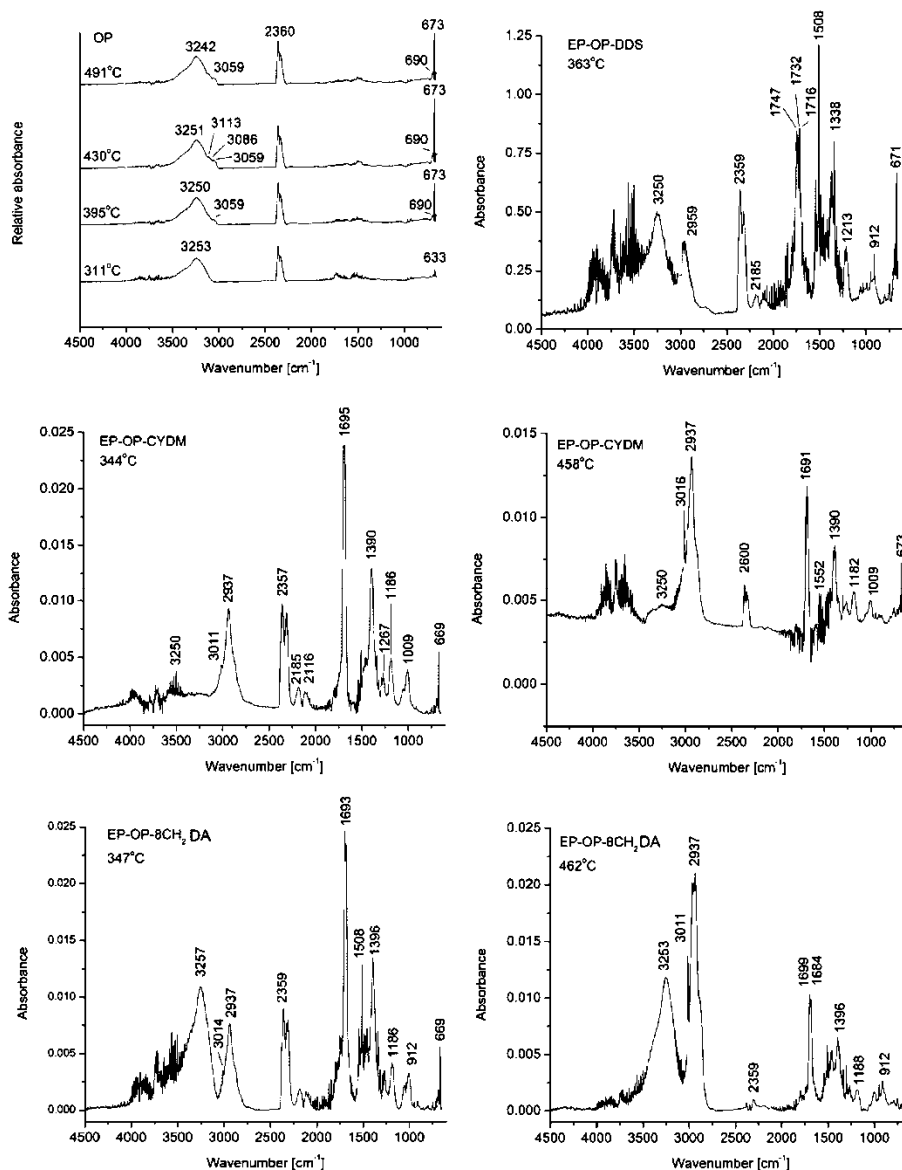


Figure 7. Gaseous FTIR spectra of the structures extracted from  $T_{\max}$  values.

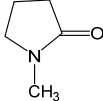
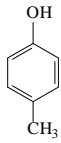
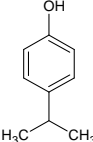
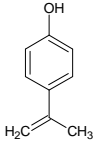
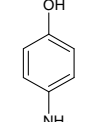
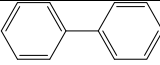
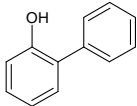
### 2.3.1.2. Py-GC-MS

The FTIR spectra offer information only concerning functional groups of the gaseous entities evolved during the decomposition of the polymer. Therefore, gas chromatography (GC) coupled with mass spectroscopy (MS) was used to identify the composition of pyrolysis (Py) products (**Py-GC-MS**). Figure 8 presents the Py-GC-MS total ion chromatograms and Table 4 shows the main identified evolved gaseous products of the S-IPNs and OP pyrolyzed at 600 °C, where +/ – denote a present/absent gaseous entity in a compound. Based on the data in Figure 8 and Table 4, a simplified thermal degradation mechanism for the S-IPNs (EP-OP-CYDM, as an exemplification) was proposed in Scheme 2. The NIST mass spectral database and prior published literature were used to identify the pyrolyzates from their mass spectra and retention times. By analyzing the total ion chromatogram (TIC) of the OP one may observe a series of pyrolyzates identified at different retention times (RT). This aspect indicates the presence of a complex gaseous mixture evolved during the OP and S-IPNs decomposition, comprised of: p-xylene (RT = 2.74 min; m/z = 91; abundance (a) =  $5.47 \times 10^5$ ); aniline (RT = 3.46 min; m/z = 93, 92, 66, 65; a =  $1.21 \times 10^6$ ) + phenol + phenyl phosphonic acid (RT = 3.59 min; m/z = 94, 92, 66, 65; 174, 94, 66, 9; a =  $4.1 \times 10^5$ ) and N-methyl-1-pyrrolidone as solvent (NMP) (RT = 3.88 min; m/z = 99, 98, 44, 42, 41; a =  $3.42 \times 10^6$ ). As observed, the predominantly aromatic structure of OP generated mostly aromatic pyrolyzates upon degradation, such as p-aminophenol, biphenyl (RT = 5.93 min; m/z = 154, 153, 152; a =  $4.9 \times 10^5$ ) and 2-phenylphenol (RT = 6.64 min; m/z = 170, 169, 167, 141, 115; a =  $1.44 \times 10^6$ ). Phenyl phosphonic acid also originates from the OP, since it is the sole compound containing phosphorus. The peak of phenyl phosphonic acid is partially merged with the high peak corresponding to phenol. Phenyl phosphonic acid may be generated through cleavage of the Ar-O bond in the OP main chain, hydrogen atoms and hydroxyl groups transfer. P-aminophenol, biphenyl and 2-phenylphenol appear at higher temperatures (higher RTs) [25]. The gaseous fragments specific to the OP, mostly phenols, do not appear in the case of the S-IPNs. This is in good agreement with the TGA data where the decrease in rate of volatiles formation (increased char formation) was observed, due to the compactness of the S-IPNs by the significant broadening of the  $T_{endset} - T_{5\%}$  range. The common gaseous fragments evolved during the thermal degradation of the S-IPNs correspond well with the components of epoxy resin, while the slight differences between the samples may arise from the structures of the curing agents. Literature data shows that bisphenol A and aromatic amines are formed during the thermal decomposition of epoxy resins crosslinked with aromatic amine hardeners [26,27]. Table 4 and Scheme 2 indicate entities similar to those reported in the literature. Since the degradation occurs in the presence of phosphoric derivatives, the phosphorus radicals play a crucial role in the reduction of released heat.

The presented data shows that the identified gaseous fragments may be classified into several groups: (1) low molecular weight entities (e.g. PO, CO, CO<sub>2</sub>, H<sub>2</sub>O – identified in the TGA-FTIR spectra); (2) cleaved fragments from main chains and subsequent rearrangements (i.e. aromatic: hydrocarbons and amines); (3) entities formed by molecular fragments reorganization at high temperatures. The composition, abundance and distribution of the pyrolyzates indicate that all samples undergo thermal degradation through initiation by random cleavages in the main chains. These scissions generate chain free radicals and carbon oxides, involving hydrogen transfer processes.

**Table 4.** Main pyrolysis products identification.

No.	Retention time (min)	Name	Mass	Ions (m/z)	Structure	EP-OP-DDS	EP-OP-CYDM	EP-OP-8CH <sub>2</sub> DA	OP
1	2.73–3	p-xylene (pX)	91	91		+	+	+	+
2	3.46-3.61	aniline (An)	93	93; 92; 66; 65		+	+	+	+
3		phenol (P)	94	94; 93; 66; 92; 65;		+	+	+	+
4		phenyl phosphonic acid (pHpPA)	158	158		+	+	+	+

5	3.88-3.98	<i>N</i> -methyl-1- pyrrolidone (NMP)	99	99; 98; 44; 42; 41		+	+	+	+
6	3.97-3.99	4-methylphenol (4MPH)	108	108; 107		+	+	+	-
7	5.02-5.05	4-(1-methylethyl)phenol (4-1MEPh)	136	121; 136		+	+	+	-
8	5.47	<i>p</i> -isopropenylphenol (pIpPh)	134	134; 119; 91		+	-	-	-
9	5.36+5.40	<i>p</i> -aminophenol (pAph)	109	109		-	-	-	+
10	5.93	biphenyl (bP)	154	154; 153; 152		-	-	-	+
11	6.64	2-phenylphenol (2PPh)	170	170; 169; 167; 141; 115		-	-	-	+

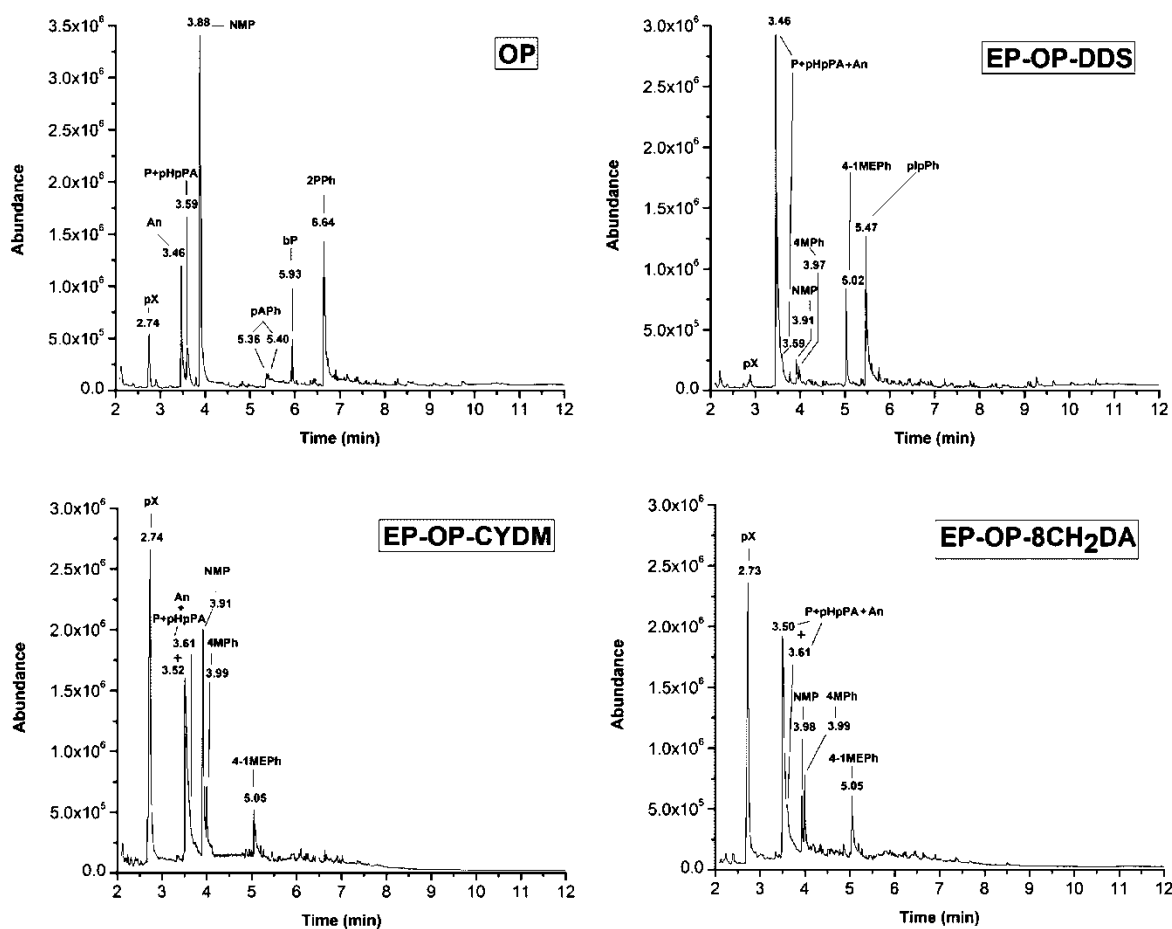
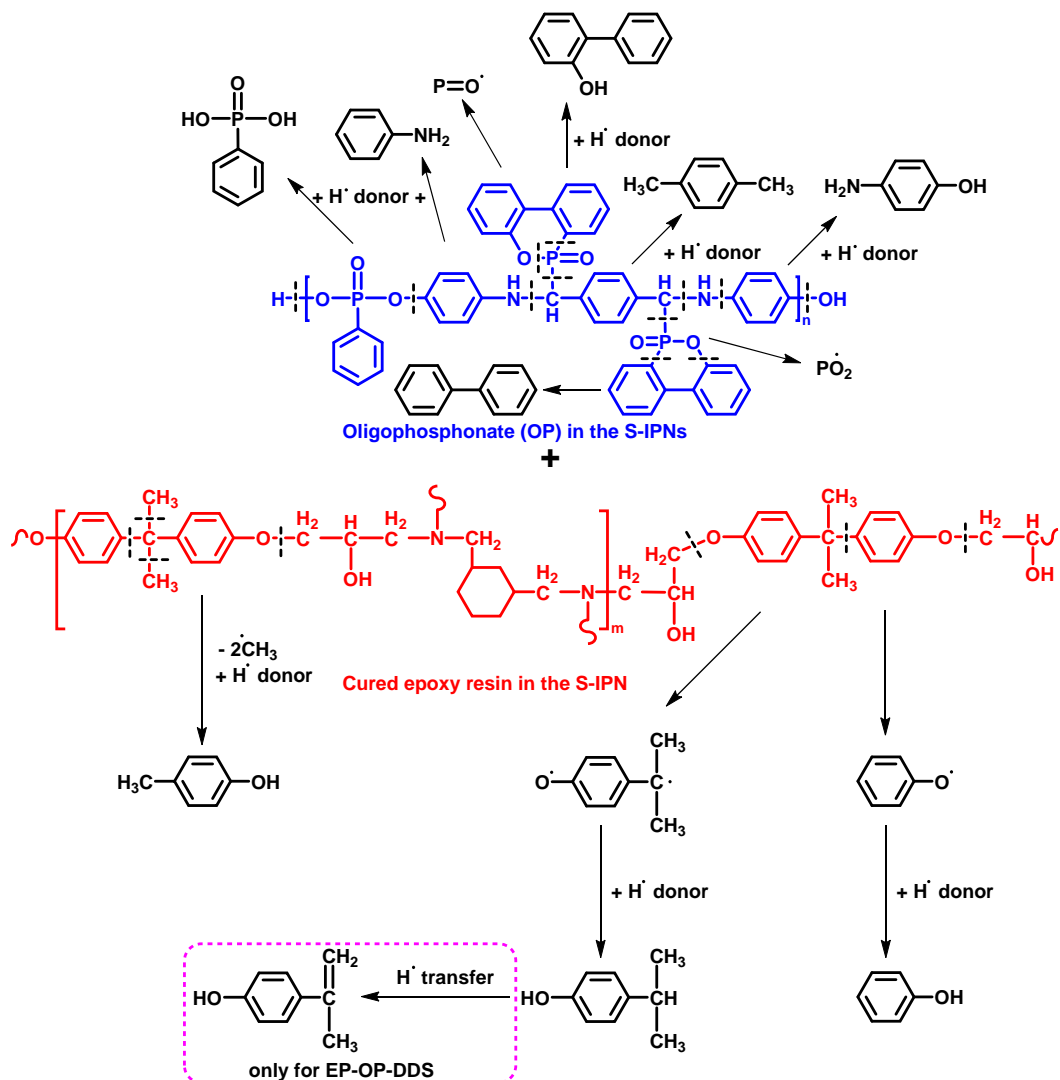


**Figure 8.** The total ion chromatograms of the S-IPNs recorded at 600°C.



**Scheme 2.** Oversimplified proposed thermal decomposition mechanism of the OP/S-IPN.

### 2.3.1.3. Flame resistance study by microscale cone calorimetry (MCC) and UL-94 VB small scale fire test

MCC is an important method in evaluating the combustion behavior of polymers, providing indispensable information regarding fire risks through parameters like: the heat release rate (**HRR**), peak of heat release rate (**p-HRR**), total heat release (**THR**) and char yield. By integrating the HRR over the entire time range (convert into temperature in Figure 9) the total heat capacity (THC) values are obtained. Table 5 shows these main combustion parameters for various formulations. From the data in Table 5 one may observe that the OP exhibited the lowest values for all parameters, while leaving the highest residue value (35.03 %). This is in a good agreement with the TGA data. The enhanced flame resistant capacity of the S-IPNs resides in lower THR values and significantly lower HRC and p-HRR values compared to OP free cured matrices. For example, p-HRR values decrease with 55.4 % (EP-OP-CYDM vs. EP-CYDM), 38.9 % (EP-OP-8CH<sub>2</sub>DA vs. EP-8CH<sub>2</sub>DA) and 33.08 % (EP-OP-DDS vs. EP-DDS). From a practical standpoint, such reduction in the peak heat release rate increases the time of escaping during a fire incident. The HRR curve shape of the OP showed a wide peak with a reduced shoulder at low temperature values (Figure 9). The shoulder appears due to the combustion behavior of the OP. During combustion OP generates a thin unstable carbonaceous layer further eliminated at higher temperatures by the vigorous gases evolution [12]. This transition disappears after introducing the OP into the S-IPNs. On close analysis of MCC data, it may be considered that the EP-OP-CYDM and EP-OP-DDS formulations have comparable parameters, the THR being much lower for the latter. EP-OP-DDS yields the highest char residue values and a superior thermal stability compared to EP-OP-CYDM, also in accordance with TGA, DSC and morphological analyses. The EP-OP-DDS is also the sole formulation to achieve a V-0 rating, while the other structures showed no classification (NC), even the two S-IPNs with the same phosphorus concentration. A content of 2 % phosphorus is not enough to achieve a V-0 rating for the S-IPNs cured with the cycloaliphatic and aliphatic hardener. This aspect may be explained by

the fact that the aliphatic hardeners's polymer chains contain an increased number of methylene ( $-\text{CH}_2-$ ) groups which decompose and release the corresponding hydrocarbon gases at specific temperatures, thus lowering their thermal stability and char yield [28]. The actual contribution of the cycloaliphatic and aliphatic curing agents to improve the flame retardancy of the epoxy resin is limited. Based on this observation, the EP-OP-DDS S-IPN may be considered the most suitable candidate to use in various applications. The higher content of phosphorus rich char within the S-IPNs, as compared to their virgin counterparts, suggests the condensed phase flame retardant mechanism.

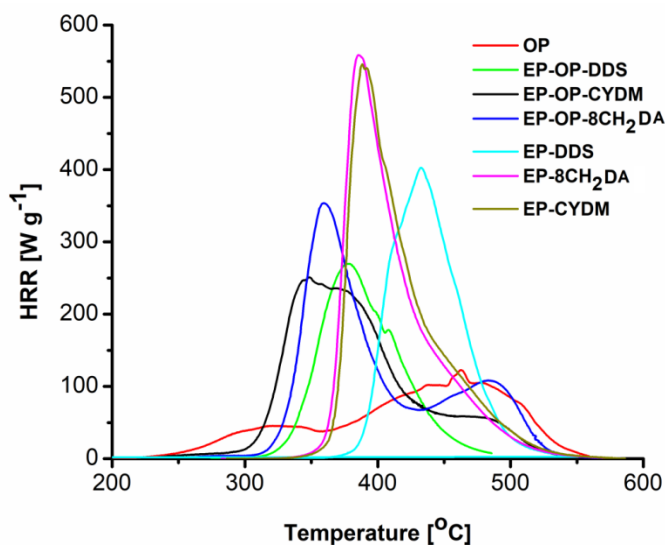


Figure 9. HRR of the OP and networks.

Table 5. UL-94 VB classification and MCC parameters of the OP and networks.

Sample	UL-94 VB	THR <sup>a</sup> (kJ g <sup>-1</sup> )	HRC <sup>b</sup> (J g <sup>-1</sup> K <sup>-1</sup> )	p-HRR <sup>c</sup> (W g <sup>-1</sup> )	W <sub>600 °C</sub> <sup>d</sup> (%)
OP	–	17.70	125.67	116	35.03
EP-OP-DDS	V-0	19.13	270.33	269	23.63
EP-OP-CYDM	NC	25.50	250.33	256	7.41
EP-OP-8CH <sub>2</sub> DA	NC	26.53	347.67	352	5.56
EP-DDS	NC	24.7	411.33	402	12.02
EP-CYDM	NC	30.93	560.67	574	4.87
EP-8CH <sub>2</sub> DA	NC	31.53	568.33	576	4.57

<sup>a</sup>Total heat release at 600 °C; <sup>b</sup>Heat release capacity; <sup>c</sup>Heat release rate peak; <sup>d</sup>Char yield at 600 °C

## Conclusions

Flame retardant S-IPNs were obtained based on an aromatic oligophosphonate and epoxy resin cured with three different hardeners: 4,4'-diaminodiphenylsulfone, 1,3-bis(aminomethyl)cyclohexane and octamethylenediamine. Structural characterization of the S-IPNs was undertaken by FTIR and SEM-EDX analyses. The samples resistance against decay was tested against three different fungal strains. The S-IPNs exhibited very good fungistatic properties against *C. cladosporioides* and presented a general long time antifungal resistance. The S-IPNs DSC curves showed a good miscibility of the oligophosphonate in the cured epoxy resin. TGA measurements were assessed in both inert and thermo-oxidative atmospheres. The non-isothermal kinetic parameters of the thermal degradation reactions were calculated with the isoconversional methods of Friedman and Ozawa-Flynn-Wall and indicated that the structures decompose following complex mechanisms in two or three stages depending on the chemical structure of the curing agent. SEM, TGA, DSC and MCC demonstrated that S-IPNs were highly compact networks. The flame retardant capacity of the structures was assessed with the UL 94-VB burning test and MCC method. TGA-FTIR and Py-GC-MS analyses were used to determine the evolved gaseous fragments of the samples and to propose a thermal degradation mechanism. All obtained data indicated that the EP-OP-DDS system may be considered the best candidate in different areas of application. For example it could be used as/or in a flame retardant coating, due to presence of the phosphine oxide group generating miscibility and adhesion to various substrates. It also may be used as a matrix for flame

retardant composites. The obtained data demonstrated that the flame retardant mechanism of the S-IPNs occurred in both gas and condensed phase. In the gas phase, the OP yielded phosphorus containing radicals ( $\text{PO}\cdot$ ,  $\text{PO}_2\cdot$ ), acting as scavengers for active H and OH based radicals from the flame area to inhibit combustion. In the condensed phase, phenyl phosphoric acid, generated in early pyrolysis stages, promotes dehydration and carbonization of the matrix and thus leading to an increasing of the residual carbon quantity. The phosphorus rich high char layer content isolated the matrix from both heat and oxygen.

The involved research team in the project realized the following activities: monthly work sessions with team members; counseling activities for the postdoctoral and doctoral students by senior researchers; organizing panels of senior scientific team problem solving; elaboration and submitting articles for publication in ISI journals; establishing and procurement of the necessary materials for developing the research program; human resources, financial and material planning for the next stage; acquisition activity planning, preparing documentation for procurement; tracking the supply flow and the use of funds and preparing stage report 2021 (scientific, financial). In order to develop and implement management structure it was followed effective and efficient communication of administrative, technical and financial research both within the team and with the contracting authority. The entire research team was involved in drafting the report stage. It was compiled the file necessary to achieve independent financial audit in 2020–2021.

**Three articles have been published and one accepted for publication, all in ISI journals. One article is in writing process. Members of the research team attended three international conferences with three oral communications and four posters. Project database has been updated and can be seen at: <https://www.icmpp.ro/epoxyphosdeg/>. The research team has met its objectives with a total degree of achievement.**

Project Manager,  
Dr. Varganici Cristian-Dragos

## References

- [1] M. Freemantle, *Chem. Eng. News* 78 (2000) 39–45; [2] P.L. Meredith, *J. Polym. Sci. Part A: Polym. Chem.* 38 (2000) 667–678; [3] J. Fan, X. Hu, C.Y. Yue, *Polym. Int.* 52 (2003) 15–22; [4] Y.J. Kou, W.Y. Zhou, B. Li, L. Dong, Y.E. Duan, Q.W. Hou, X.R. Liu, H.W. Cai, Q.G. Chen, Z.M. Dang, *Compos. Part. A. Appl. Sci.* 114 (2018) 97–106; [5] M. Laurien, B. Demir, H. Buttemeyer, A.S. Herrmann, T.R. Walsh, L.C. Ciacchi, *Macromol.* 51 (2018) 3983–3993; [6] M. Zhao, L.H. Meng, L.C. Ma, L.N. Ma, X.B. Yang, Y.D. Huang, J.E. Ryu, A. Shankar, T.X. Li, C. Yan, Z.H. Guo, *Compos. Sci. Technol.* 154 (2018) 28–36; [7] D. Klemperer, L.H. Sperling, L.A. Utracki, *Interpenetrating Polymer Networks*, American Chemical Society, Washington DC, 1994; [8] C. Hamciuc, T. Vlad–Bubulac, D. Serbezeanu, I.D. Carja, E. Hamciuc, G. Lisa, V. Forrat Pérez, *RSC Adv.* 6 (2016) 22764–22776; [9] R.M. Silverstein, F.S. Webster, D.J. Kiemle, *Spectrometric Identification of Organic Compounds*, Seventh ed., John Wiley & Sons, 2005; [10] G. Socrates, *Infrared and Raman Characteristic Group Frequencies: Tables and Charts*, Third ed., Wiley, Chichester, 2004, p. 366; [11] D. Rosu, L. Rosu, F. Mustata, C.D. Varganici, *Polym. Degrad. Stab.* 97 (2012) 1261–1269; [12] I.–D. Carja, D. Serbezeanu, T. Vlad–Bubulac, C. Hamciuc, A. Coroaba, G. Lisa, C.G. López, M.F. Soriano, V.F. Pérez, M.D.R. Sánchez, *J. Mater. Chem. A* 2 (2014) 16230–16241; [13] C.–D. Varganici, L. Rosu, D. Rosu, B.C. Simionescu, *Compos. Part B: Eng.* 50 (2013) 273–278; [14] D. Rosu, L. Rosu, C.–D. Varganici, *J. Anal. Appl. Pyrolysis* 100 (2013) 103–110; [15] I. Butnaru, C.–D. Varganici, M. Pinteala, S. Lehner, M. Bruma, S. Gaan, *J. Anal. Appl. Pyrolysis* 134 (2018) 254–264; [16] S. Vyazovkin, A.K. Burnham, J.M. Criado, L.A. Pérez–Maqueda, C. Popescu, N. Sbirrazzouli, *Thermochim. Acta* 5 (2011) 1–19; [17] D. Rosu, C.N. Cascavaf, C. Ciobanu, L. Rosu, *J. Anal. Appl. Pyrolysis* 72 (2004) 191–196; [18] C.–D. Varganici, D. Rosu, C. Barbu–Mic, L. Rosu, D. Popovici, C. Hulubei, B.C. Simionescu, *J. Anal. Appl. Pyrolysis* 113 (2015) 390–401; [19] M. Worzakowska, *Polymer* 48 (2007) 1148–1154; [20] M. Edelmann, M. Gedan–Smolka, G. Heinrich, D. Lehmann, *Thermochim. Acta* 452 (2007) 59–64; [21] J. Opfermann, *J. Therm. Anal. Calorim.* 60 (2000) 641–658; [22] L. Jiang, P. Zhang, L. Dong, K. Liu, *J. Therm. Anal. Calorim.* 138 (2019) 3031–3037; [23] D. Rosu, L. Rosu, M. Brebu, *J. Anal. Appl. Pyrolysis* 92 (2011) 10–18; [24] L.D. Field, H.L. Li, A.M. Magill, *Organic Structures from Spectra*, Sixth ed., John Wiley & Sons, Hoboken, 2020; [25] W. Xie, W.–P. Pan, K.C. Chuang, *J. Therm. Anal. Calorim.* 64 (2001) 477–485; [26] A. Bifulco, D. Parida, K.A. Salmeia, S. Lehner, R. Stämpfli, H. Markus, G. Malucelli, F. Branda, S. Gaan, *Compos. Part C: Open Access* 2 (2020) 100022; [27] A. Bifulco, D. Parida, K.A. Salmeia, R. Nazir, S. Lehner, R. Stämpfli, H. Markus, G. Malucelli, F. Branda, S. Gaan, *Mater. Design* 193 (2020) 108862; [28] P. Deng, Y. Liu, Y. Liu, C. Xu, Q. Wang, *Polym. Adv. Technol.* 29 (2018) 1294–1302.